HHS Public Access

Author manuscript

J Bone Miner Res. Author manuscript; available in PMC 2019 August 01.

Published in final edited form as:

J Bone Miner Res. 2018 August ; 33(8): 1513–1519. doi:10.1002/jbmr.3449.

Second-Generation SYK Inhibitor Entospletinib Ameliorates Fully Established Inflammation and Bone Destruction in the Cherubism Mouse Model

Tetsuya Yoshimoto[1], **Tatsuhide Hayashi**[1,2], **Toshio Kondo**[1,3], **Mizuho Kittaka**[1], **Ernst J Reichenberger**[4], and **Yasuyoshi Ueki**[1,5]

[1]Department of Oral and Craniofacial Sciences, School of Dentistry, University of Missouri–Kansas City (UMKC), MO, USA

[2]Department of Dental Materials Science, Aichi Gakuin University School of Dentistry, Nagoya, Japan

[3]Department of Molecular Biology and Biochemistry, Okayama University Graduate School of Medicine, Dentistry and Pharmaceutical Sciences, Okayama, Japan

[4]Department of Reconstructive Sciences, School of Dental Medicine, University of Connecticut Health, Farmington, CT, USA

[5]Center of Excellence in the Study of Dental and Musculoskeletal Tissues (CEMT), University of Missouri–Kansas City (UMKC), Kansas City, MO, USA

Abstract

Cherubism is a craniofacial disorder characterized by maxillary and mandibular bone destruction. Gain-of-function mutations in the SH3-domain binding protein 2 (SH3BP2) are responsible for the excessive bone resorption caused by fibrous inflammatory lesions. A homozygous knock-in (KI) mouse model for cherubism (*Sh3bp2*$^{KI/KI}$) develops autoinflammation resulting in systemic bone destruction. Although administration of the TNF-α blocker etanercept to neonatal *Sh3bp2*$^{KI/KI}$ mice prevented the disease onset, this therapy was not effective for adult *Sh3bp2*$^{KI/KI}$ mice or human cherubism patients who already had lesions. Because genetic ablation of spleen tyrosine kinase (SYK) in myeloid cells rescues *Sh3bp2*$^{KI/KI}$ mice from inflammation, we examined whether SYK inhibitor administration can improve fully developed cherubism symptoms in adult *Sh3bp2*$^{KI/KI}$ mice. Entospletinib (GS-9973) was intraperitoneally injected into 10-week-old *Sh3bp2*$^{KI/KI}$ mice every day for 6 weeks. Treatment with GS-9973 improved facial swelling and histomorphometric analysis of lung and liver tissue showed that GS-9973 administration significantly reduced inflammatory infiltrates associated with decreased levels of serum TNF-α Micro–computed tomography (μCT) analysis showed that GS-9973 treatment reduced bone

Address correspondence to: Yasuyoshi Ueki, MD, PhD, Department of Oral and Craniofacial Sciences, University of Missouri–Kansas City, School of Dentistry, 650 E 25th Street, Kansas City, MO 64108, USA. uekiy@umkc.edu.

Authors' roles: TY, TH, and TK performed experiments. MK, EJR, and YU designed the experiments. All authors contributed to the data analysis and interpretation of the results. TY and YU wrote the manuscript, and all authors approved the manuscript. TY and YU are responsible for the data integrity and analysis.

Disclosures

All authors declare that they have no conflicts of interest.

erosion in mandibles, calvariae, and ankle and elbow joints of *Sh3bp2*$^{KI/KI}$ mice compared to *Sh3bp2*$^{KI/KI}$ mice treated with dimethyl sulfoxide (DMSO). Taken together, the results demonstrate that administration of the SYK inhibitor ameliorates an already established cherubism phenotype in mice, suggesting that pharmacological inhibition of SYK may be a treatment option for cherubism patients with active disease progression.

Keywords

CHERUBISM; SH3BP2; SYK; ENTOSPLETINIB/GS-9973; AUTOINFLAMMATION; BONE DESTRUCTION

Introduction

Cherubism (OMIM#118400) is a genetic disorder characterized by bilateral multilocular cystic bone destruction in the maxilla and mandibula. The cystic bone lesions are filled with proliferative fibro-osseous tissue containing a large number of tartrate-resistant acid phosphatase (TRAP)-positive multinucleated giant cells. Excessive tissue proliferation at around 2 to 5 years old leads to a disfiguring swelling of the lower face reminiscent of Renaissance cherubic angels. Swelling of submandibular lymph nodes is an additional characteristic symptom of cherubism.[1] Cherubism lesions usually begin to regress after puberty by mechanisms that may involve the toll-like receptor (TLR)-myeloid differentiation primary response 88 (MYD88) pathway.[2,3] In severe cases, the lesions expand into the orbital walls or upper airway,[4–7] resulting in upward gazing, optic neuropathy,[7] or respiratory disturbance.[8] Heterozygous mutations in the RSPPDG hexapeptide sequence of the SH3-domain binding protein 2 (SH3BP2) are responsible for cherubism.[9] The mutant SH3BP2 protein escapes from poly adenosine diphosphate (ADP)-ribosylation by tankyrase that leads to proteasomal degradation; therefore, increased amounts of mutant SH3BP2 protein promote macrophage and osteoclast activation in a gain-of-function manner.[10,11] The homozygous cherubism knock-in (KI) mouse model carrying a typical SH3BP2 mutation spontaneously develops systemic macrophage inflammation starting at around 1 week of age in a TNF-α-dependent manner[12,13] and exhibits joint destruction as well as jawbone erosion by osteoclasts.[13] Because inflammatory lesions in *Sh3bp2*$^{KI/KI}$ mice develop in the absence of T and B cells, cherubism is considered a new form of autoinflammatory disease.[13,14]

We have previously shown that postnatal administration of the TNF-α blocker etanercept is able to prevent the development of inflammation when administered to the inflammation-free neonatal (1-week-old) *Sh3bp2*$^{KI/KI}$ mice.[12] However, the effect was very limited when it was administered to 10-week-old *Sh3bp2*$^{KI/KI}$ mice with fully active inflammation.[12] These results suggest that anti-TNF-α therapy may be effective in young cherubism patients, if treated before the inflammatory phase or bone resorption occurs, but not in patients who are in the active and destructive phase of the disease. In agreement with the observation in mice, treatment with TNF-α antagonist adalimumab was not effective in two cases of active cherubism.[15] Recent studies showed clinical and functional improvement in a patient with aggressive cherubism treated with the calcineurin inhibitor tacrolimus, suggesting that

blocking of NFAT-mediated transcriptional activation might prevent the need for surgical removal of growing lesions and recurring maxillofacial surgeries for severe cherubism.[16] However, more clinical trials are necessary to confirm the efficacy and safety of tacrolimus for mild and severe cherubism.

Spleen tyrosine kinase (SYK) is a cytoplasmic protein tyrosine kinase predominantly expressed in the hematopoietic cell lineage. SYK signaling evokes diverse biologic functions particularly in B cells, neutrophils, macrophages, mast cells, and osteoclasts by coupling immune cell receptors to intracellular signaling pathways.[17] Thus, SYK has been a promising drug target for immune and inflammatory disorders.[18] Because SYK is a key mediator of mutant SH3BP2 in myeloid cells and because genetic depletion of SYK in the myeloid cell lineage rescues inflammation in *Sh3bp2*$^{KI/KI}$ mice,[2,19] we examined whether pharmacological inhibition of SYK improves cherubism symptoms in adult *Sh3bp2*$^{KI/KI}$ mice that are in active disease status. Here, we show that administration of the novel SYK inhibitor GS-9973 ameliorates inflammation and bone destruction in adult cherubism mice.

Materials and Methods

Animals

Cherubism mice (*Sh3bp2*$^{KI/KI}$) on C57BL/6 background carrying the most common P418R mutation in human cherubism (P416R in mice) have been described.[13] All mice were bred under specific-pathogen-free conditions. All animal experiments were approved by the Institutional Animal Care and Use Committee at the University of Missouri–Kansas City.

SYK inhibitor administration

Entospletinib (GS-9973, MedChem Express) diluted with dimethyl sulfoxide (DMSO) was intraperitoneally injected into male and female *Sh3bp2*$^{KI/KI}$ and wild-type control mice (*Sh3bp2*$^{+/+}$) every day for 6 weeks from 10 weeks of age (100 mg/kg) or for 7 weeks from 1 week of age (50 mg/kg; Supplemental Fig. 5).

Micro–computed tomography analysis

Tissues including mandible, calvaria, femur, and elbow and ankle joints were fixed with 4% paraformaldehyde (PFA)/phosphate buffered saline (PBS) for 24 hours and soaked in 70% ethanol for a scan with the Skyscan1174 (Bruker, Kontich, Belgium) under the following conditions: 80 kV X-ray energy, 6.67 μm pixel size (mandible, femur, and elbow and ankle joints) or 11.6 μm pixel size (calvaria), and 0.4-degree rotation step with 3000 ms exposure time. Scanned data were reconstructed with NRecon software (Bruker) with dynamic ranges as follows: 0 to 0.14 (elbow joint), 0 to 0.15 (ankle joint), 0 to 0.16 (femur), 0 to 0.18 (calvaria), or 0 to 0.22 (mandible). Three-dimensional (3D) images were created using CTVox software (Bruker).

Quantification of bone properties

Reconstructed data with NRecon were segmented by CTAn software (Bruker) to define the region of interest in each tissue. Distance between the cementoenamel junction (CEJ) and alveolar bone crest (ABC) at the distal lingual surface of mandibular first molar (M1) was

measured in reconstructed 2D images with CTAn software. The region for alveolar bone volume analysis comprised 15 slices of the furcation area underneath the M1. Calcaneus bone volume was used for quantitative assessment of bone erosion in ankle joints. Calvarial micro– computed tomography (μCT) images (6 mm × 6 mm) were used to calculate the erosion area (%) and bone surface/bone volume (BS/BV). The intersection of coronal and sagittal sutures was used as the center position. The total area of bone erosion including suture area in 6-mm × 6-mm calvarial bone images was measured as pixels with ImageJ software (NIH, Bethesda, MD, USA; https://imagej.nih.gov/ij/) and divided by the total number of pixels. The region for trabecular bone analysis comprised 1 mm (151 slices) of the distal femur beneath the growth plate. The region for cortical bone analysis comprised 100 slices at the midshaft of the femur. Results from right and left bones were averaged in each mouse except for calvariae.

Histological analysis

Postmortem tissues were fixed with 4% PFA/PBS for 1 day before paraffin embedding. Sections (6 μm) were stained with hematoxylin and eosin (H&E).

RNA and quantitative PCR analysis

Total RNA from liver tissue extracted with Ribozol (VWR) was transcribed to cDNA using the High Capacity cDNA Reverse Transcription Kit (Life Technologies). Quantitative PCR (qPCR) reactions were performed with the StepOne Plus system (Life Technologies) using Maxima SYBR Green mix (Thermo Fisher). Relative gene expression levels were calculated using a relative standard curve method to compare *TNF-α* expression levels in whole liver tissue. Results were normalized by *Gapdh* expression levels. qPCR primers used in this study are: Tnfα-F 5′-GATCGGTCCCCAAAGGGATG-3′, Tnfα-R 5′TGTGAGGGTCTGGGCCATAG-3′; Gapdh-F 5′-ATCAAGAAGGTGGTGAAGCA-3′, Gapd h-R 5′-GACAACCTGGTCCTCAGTGT-3′.

Histomorphometry

Total inflammatory area in liver and lung sections stained with H&E was measured as pixels with ImageJ, which was divided by total pixels of the entire tissue to calculate the proportion of inflammatory area (%).[(2)] For the liver measurement, vasculature areas were excluded. Lung and liver images were taken with 1× or 4× objectives, respectively (Nikon E800). Results from four to five images from different areas of each tissue section were averaged.

Serum ELISA

Mouse TNF-α Duo-Set ELISA kit (R&D Systems, Minneapolis, MN, USA) was used. Serum was separated from blood with Vacutainer collection tube (BD) and stored at –80°C until use.

Statistics

Statistical analysis was performed by the two-tailed unpaired Student's *t* test to compare two groups or by one-way ANOVA with Tukey-Kramer post hoc test to compare three or more groups (GraphPad Prism 5; GraphPad Software, Inc., La Jolla, CA, USA). Values of $p < 0.05$

were considered to be significant. Average ± SD numbers for each graph are listed in Supplemental Table 1.

Results and Discussion

GS-9973 administration suppresses fully developed inflammation in *Sh3bp2*$^{KI/KI}$ mice

We chose the SYK inhibitor entospletinib (GS-9973), because this second-generation compound has greater selectivity against SYK than tamatinib (R406), which is the active metabolite of fostamatinib (R788)[20–23] and has a longer half-life in mouse plasma compared to R406.[21,24] Although GS-9973 has relatively high selectivity to tyrosine kinase non-receptor 1 (TNK1, Kd (dissociation constant): TNK1 86 nM versus SYK 10.5 nM),[20,22] the most comprehensive clinical experience of SYK inhibitors to date has been obtained with GS-9973.[23,25] GS-9973 is currently in clinical trials for certain types of leukemia and lymphoma (https://clinicaltrials.gov).

To address the therapeutic effect of GS-9973 on cherubism mice, 10-week-old *Sh3bp2*$^{KI/KI}$ mice were intraperitoneally injected with GS-9973 (100 mg/kg) every day for 6 weeks. Results were compared to *Sh3bp2*$^{KI/KI}$ mice injected with vehicle (DMSO) (Fig. 1A). GS-9973 treatment rescued the closure of eyelids associated with facial skin inflammation in all male and female *Sh3bp2*$^{KI/KI}$ mice (Fig. 1B, red arrows), which had not improved in *Sh3bp2*$^{KI/KI}$ mice treated with DMSO (Fig. 1B, blue arrows). Consistent with this observation, body weight loss was prevented in the *Sh3bp2*$^{KI/KI}$ mice treated with GS-9973 compared to DMSO-treated *Sh3bp2*$^{KI/KI}$ mice (Fig. 1C).

Inflammatory infiltrates in the lung and liver are other characteristics of *Sh3bp2*$^{KI/KI}$ mice.[13] Therefore, we examined whether GS-9973 treatment can also reduce the development of inflammation in lung and liver. GS-9973 administration in *Sh3bp2*$^{KI/KI}$ mice significantly reduced the number of inflammatory nodules compared to the DMSO-treated *Sh3bp2*$^{KI/KI}$ mice (Fig. 1D), which was confirmed by histomorphometric analysis measuring the total inflammatory area against total lung area (Fig. 1E). In the liver, GS-9973 administration effectively reduced the total area of macrophage-rich inflammation compared to DMSO-treated *Sh3bp2*$^{KI/KI}$ mice (Fig. 1F, G). Consistent with the decreased inflammatory infiltrates, expression levels of TNF-α mRNA in liver tissue were significantly suppressed in GS-9973-treated *Sh3bp2*$^{KI/KI}$ mice (Fig. 1H). Finally, serum TNF-α levels in *Sh3bp2*$^{KI/KI}$ mice were markedly decreased in GS-9973-treated *Sh3bp2*$^{KI/KI}$ mice (Fig. 1I) and GS-9973 treatment suppressed TNF-α mRNA levels in bone marrow–derived M-CSF-dependent macrophages (BMMs) (Supplemental Fig. 1). Taken together, these results suggest that the SYK inhibitor treatment ameliorates fully developed inflammation in *Sh3bp2*$^{KI/KI}$ mice by suppressing macrophage activation.

GS-9973 administration rescues *Sh3bp2*$^{KI/KI}$ mice from inflammatory bone destruction

We next examined whether GS-9973 treatment rescues bone erosion and bone loss in *Sh3bp2*$^{KI/KI}$ mice. μCT images of mandibular bone surface of *Sh3bp2*$^{KI/KI}$ mice treated with GS-9973 showed reduced erosion pit formation compared to *Sh3bp2*$^{KI/KI}$ mice treated with DMSO (Fig. 2A, top). Alveolar bone loss was also suppressed in the treated mice (Fig.

2A, bottom). To confirm the rescue from jawbone loss, the distance between CEJ and ABC at the distal lingual surface of the mandibular first molar was measured using reconstructed 2D μCT images. GS-9973 administration significantly contributed to the reduction in average CEJ-ABC distance (Fig. 2B). Increase in alveolar bone volume/tissue volume (BV/TV) was also significant (Fig. 2C). Reduction rate of alveolar BV/TV in GS-9973-treated *Sh3bp2*$^{KI/KI}$ mice compared to *Sh3bp2*$^{+/+}$ mice treated with DMSO was in average 4.1-fold smaller than in DMSO-treated *Sh3bp2*$^{KI/KI}$ mice (Fig. 2D).

Consistent with reduced erosion pit numbers on calvarial bone surfaces (Fig. 2E), total bone erosion areas on calvariae were significantly reduced in *Sh3bp2*$^{KI/KI}$ mice treated with GS-9973 compared to *Sh3bp2*$^{KI/KI}$ mice treated with DMSO (Fig. 2F). Bone surface/bone volume (BS/BV), a parameter for bone surface roughness, of calvarial bone was decreased in GS-9973-treated *Sh3bp2*$^{KI/KI}$ mice compared to DMSO-treated *Sh3bp2*$^{KI/KI}$ mice (Fig. 2G). Consistent with the results, BV/TV of calvarial bone was increased in GS-9973-treated *Sh3bp2*$^{KI/KI}$ mice (Fig. 2H).

Because *Sh3bp2*$^{KI/KI}$ mice develop bone-destructive synovial tissue inflammation in the elbow and knee joints,[12,13] we further investigated whether GS-9973 administration amelio-rates inflammatory bone destruction. μCT analysis of *Sh3bp2*$^{KI/KI}$ mice treated with GS-9973 revealed obvious rescue from bone destruction in ankle joints (Fig. 2I) and elbow joints with improved coronoid fossa appearance (Supplemental Fig. 2). To quantify the rescue from focal bone destruction, BV and BV/TV of the calcaneus in GS-9973-treated *Sh3bp2*$^{KI/KI}$ mice were compared to those in DMSO-treated *Sh3bp2*$^{KI/KI}$ mice. GS-9973 administration significantly increased the average BV and BV/TV (Fig. 2J and K, respectively). Reduction rate of calcaneus BV/TV in GS-9973-treated *Sh3bp2*$^{KI/KI}$ mice compared to *Sh3bp2*$^{+/+}$ mice treated with DMSO was in average 2.9-fold smaller than in DMSO-treated *Sh3bp2*$^{KI/KI}$ mice (Fig. 2L).

Bone property analysis of femurs from GS-9973-treated *Sh3bp2*$^{KI/KI}$ mice showed a significant increase in cortical bone thickness (Cort.Th), cortical bone mineral density (Cort.BMD), and cortical bone volume (Cort.BV) at the midshaft compared to DMSO-treated *Sh3bp2*$^{KI/KI}$ mice, while those values were still less than GS-9973-treated or DMSO-treated *Sh3bp2*$^{+/+}$ mice (Supplemental Fig. 3A-D). On the other hand, there were no changes in trabecular BV/TV, trabecular bone thickness (Tb.Th), trabecular bone number (Tb.N), and trabecular bone separation (Tb.Sp) at the distal femur compared to DMSO-treated *Sh3bp2*$^{KI/KI}$ mice (Supplemental Fig. 3E-I). These data suggest that GS-9973 treatment in *Sh3bp2*$^{KI/KI}$ mice is effective in the treatment of alveolar and calvarial bone loss and partially effective in improving systemic bone loss and that cortical bone resorption is more susceptible to the SYK inhibitor. Treatment of *Sh3bp2*$^{KI/KI}$ BMMs and *Sh3bp2*$^{KI/KI}$ mice with GS-9973 suppressed osteoclast formation (Supplemental Fig. 4A-D), suggesting that decreased osteoclast differentiation under suppressed macrophage inflammation is the major cause of improved bone destruction in *Sh3bp2*$^{KI/KI}$ mice. Interestingly, *Sh3bp2*$^{KI/KI}$ BMMs and *Sh3bp2*$^{KI/KI}$ mice were more susceptible to GS-9973 than *Sh3bp2*$^{+/+}$ BMMs and *Sh3bp2*$^{+/+}$ mice, respectively (Supplemental Fig. 4A-D). The increased susceptibility of *Sh3bp2*$^{KI/KI}$ BMMs was also observed in *TNF-α* expression (Supplemental Fig. 1). Finally,

we confirmed that similar to the treatment with etanercept,[12] GS-9973 treatment of 1-week-old *Sh3bp2*$^{KI/KI}$ mice prevents autoinflammatory response (Supplemental Fig. 5).

In summary, we demonstrated that the novel SYK inhibitor GS-9973 ameliorates fully developed inflammation and bone destruction in the mouse model of cherubism. Anti-SYK therapy should be considered a potential strategy for pharmacological treatment of human cherubism patients particularly during aggressive and destructive phases of the disease. In fact, because GS-9973 is orally effective,[21] oral administration may be a clinical preference for treatment of cherubism patients. Effectiveness of GS-9973 in cherubism treatment may expand the applicability of SYK inhibitors to autoinflammatory disorders.

Supplementary Material

Refer to Web version on PubMed Central for supplementary material.

Acknowledgments

Research reported in this publication was supported by the NIH (National Institute of Dental and Craniofacial Research [NIDCR], R01DE025870 to YU; National Institute of Arthritis and Musculoskeletal and Skin Diseases [NIAMS], R21AR070953 to YU). The content is solely the responsibility of the authors and does not necessarily represent the official views of the NIH. TY is a recipient of the Japan Society for the Promotion of Science (JSPS) overseas research fellowship. TH is a recipient of a research fellowship from Aichi Gakuin University. MK is a recipient of a fellowship from the brain circulation program to develop new leaders for international dental education course through international collaborative dental research, Japan, and of a fund for young researchers from Japanese Society of Periodontology. We thank all members of the Bone Biology Research Program at the University of Missouri–Kansas City, School of Dentistry for suggestions and critical comments.

References

1. Reichenberger EJ, Levine MA, Olsen BR, Papadaki ME, Lietman SA. The role of SH3BP2 in the pathophysiology of cherubism. Orphanet J Rare Dis 2012;7 Suppl 1:S5. [PubMed: 22640988]
2. Yoshitaka T, Mukai T, Kittaka M, et al. Enhanced TLR-MYD88 signaling stimulates autoinflammation in SH3BP2 cherubism mice and defines the etiology of cherubism. Cell Rep 2014;8(6):1752–66. [PubMed: 25220465]
3. Prod'Homme V, Boyer L, Dubois N, et al. Cherubism allele heterozygosity amplifies microbe-induced inflammatory responses in murine macrophages. J Clin Invest 2015 4;125 (4):1396–400. [PubMed: 25705883]
4. Hawes MJ. Cherubism and its orbital manifestations. Ophthal Plast Reconstr Surg 1989;5(2):133–40.
5. Colombo F, Cursiefen C, Neukam FW, Holbach LM. Orbital involvement in cherubism. Ophthalmology 2001;108(10):1884–8. [PubMed: 11581066]
6. Carroll AL, Sullivan TJ. Orbital involvement in cherubism. Clin Exp Ophthalmol 2001;29(1):38–40. [PubMed: 11272784]
7. Ahmadi AJ, Pirinjian GE, Sires BS. Optic neuropathy and macular chorioretinal folds caused by orbital cherubism. Arch Ophthalmol 2003;121(4):570–3. [PubMed: 12695257]
8. Battaglia A, Merati A, Magit A. Cherubism and upper airway obstruction. Otolaryngol Head Neck Surg 2000;122(4):573–4. [PubMed: 10740181]
9. Ueki Y, Tiziani V, Santanna C, et al. Mutations in the gene encoding c-Abl-binding protein SH3BP2 cause cherubism. Nat Genet 2001;28(2):125–6. [PubMed: 11381256]
10. Levaot N, Voytyuk O, Dimitriou I, et al. Loss of tankyrase-mediated destruction of 3BP2 is the underlying pathogenic mechanism of cherubism. Cell 2011;147(6):1324–39. [PubMed: 22153076]

11. Guettler S, LaRose J, Petsalaki E, et al. Structural basis and sequence rules for substrate recognition by tankyrase explain the basis for cherubism disease. Cell 2011;147(6):1340–54. [PubMed: 22153077]
12. Yoshitaka T, Ishida S, Mukai T, Kittaka M, Reichenberger E, Ueki Y. Etanercept administration to neonatal SH3BP2 knock-in cherubism mice prevents TNF-α-induced inflammation and bone loss. J Bone Miner Res 2014;29(5):1170–82. [PubMed: 24978678]
13. Ueki Y, Lin CY, Senoo M, et al. Increased myeloid cell responses to M-CSF and RANKL cause bone loss and inflammation in SH3BP2 "cherubism" mice. Cell 2007;128(1):71–83. [PubMed: 17218256]
14. Masters SL, Simon A, Aksentijevich I, Kastner DL. Horror auto-inflammaticus: the molecular pathophysiology of autoinflammatory disease. Annu Rev Immunol 2009;27:621–68. [PubMed: 19302049]
15. Hero M, Suomalainen A, Hagstrom J, et al. Anti-tumor necrosis factor treatment in cherubism - clinical, radiological and histological findings in two children. Bone 2013;52(1):347–53. [PubMed: 23069372]
16. Kadlub N, Vazquez MP, Galmiche L, et al. The calcineurin inhibitor tacrolimus as a new therapy in severe cherubism. J Bone Miner Res 2015;30(5):878–85. [PubMed: 25491283]
17. Mocsai A, Ruland J, Tybulewicz VL. The SYK tyrosine kinase: a crucial player in diverse biological functions. Nat Rev Immunol 2010; 10(6):387–402. [PubMed: 20467426]
18. Geahlen RL. Getting Syk: spleen tyrosine kinase as a therapeutic target. Trends Pharmacol Sci 2014;35(8):414–22. [PubMed: 24975478]
19. Mukai T, Ishida S, Ishikawa R, et al. SH3BP2 cherubism mutation potentiates TNF-αlpha-induced osteoclastogenesis via NFATc1 and TNF-αlpha-mediated inflammatory bone loss. J Bone Miner Res 2014;29 (12):2618–35. [PubMed: 24916406]
20. Burke RT, Meadows S, Loriaux MM, et al. A potential therapeutic strategy for chronic lymphocytic leukemia by combining Idelalisib and GS-9973, a novel spleen tyrosine kinase (Syk) inhibitor. Oncotarget 2014;5(4):908–15. [PubMed: 24659719]
21. Currie KS, Kropf JE, Lee T, et al. Discovery of GS-9973, a selective and orally efficacious inhibitor of spleen tyrosine kinase. J Med Chem 2014;57(9):3856–73. [PubMed: 24779514]
22. Sharman J, Hawkins M, Kolibaba K, et al. An open-label phase 2 trial of entospletinib (GS-9973), a selective spleen tyrosine kinase inhibitor, in chronic lymphocytic leukemia. Blood 2015;125 (15):2336–43. [PubMed: 25696919]
23. Liu D, Mamorska-Dyga A. Syk inhibitors in clinical development for hematological malignancies. J Hematol Oncol 2017;10(1):145. [PubMed: 28754125]
24. Suljagic M, Longo PG, Bennardo S, et al. The Syk inhibitor fostamatinib disodium (R788) inhibits tumor growth in the Emu-TCL1 transgenic mouse model of CLL by blocking antigen-dependent B-cell receptor signaling. Blood 2010;116(23):4894–905. [PubMed: 20716772]
25. Sharman J, Di Paolo J. Targeting B-cell receptor signaling kinases in chronic lymphocytic leukemia: the promise of entospletinib. Ther Adv Hematol 2016;7(3):157–70. [PubMed: 27247756]

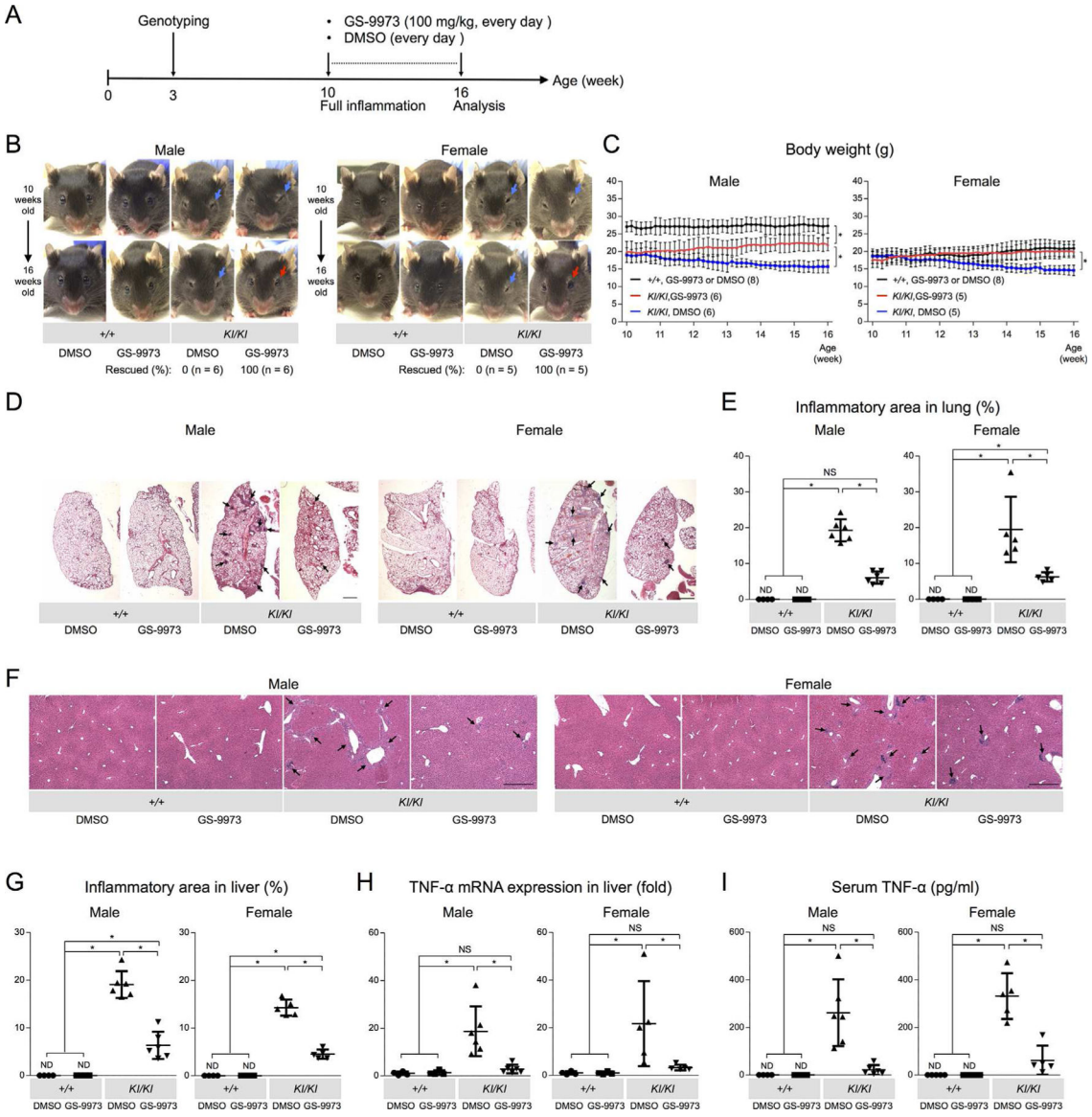

Fig. 1.

GS-9973 administration to actively inflamed 10-week-old *Sh3bp2*$^{KI/KI}$ mice improves facial swelling, body weight loss, and systemic autoinflammation. (*A*) Experimental sequence of GS-9973 administration. 10-week-old *Sh3bp2*$^{+/+}$ and *Sh3bp2*$^{KI/KI}$ mice were treated with 100 mg/kg of GS-9973 or DMSO every day for 6 weeks. Mice were euthanized at 16 weeks of age for analysis. (*B*) Facial appearance of GS-9973- treated or DMSO-treated mice (top: before treatment at 10 weeks of age; bottom: after treatment at 16 weeks of age). Blue arrows indicate closed eyelids due to facial skin inflammation. GS-9973 treatment improved eyelid closure in *Sh3bp2*$^{KI/KI}$ mice at 16 weeks old (red arrows). Numbers represent the percentage of *Sh3bp2*$^{KI/KI}$ mice with improved facial swelling. (*C*) Body weight changes in GS-9973-administered or DMSO-administered *Sh3bp2*$^{+/+}$ and *Sh3bp2*$^{KI/KI}$ mice. Body weight in GS-9973-administered *Sh3bp2*$^{KI/KI}$ mice (red lines) was increased, whereas weight of DMSO-administered *Sh3bp2*$^{KI/KI}$ mice (blue lines) continued to decrease.

Numbers in parentheses represent the number of the mice weighed. (*D*) H&E-stained lung tissue sections. Arrows indicate inflammatory nodules. Scale bar = 1 mm. (*E*) Quantitative analysis of total inflamed area in the lung. (*F*) Liver sections from GS-9973-treated or DMSO-treated *Sh3bp2*$^{+/+}$ and *Sh3bp2*$^{KI/KI}$ mice (H&E). Arrows indicate inflammatory infiltrates. Scale bar = 500 μm. (*G*) Quantitative measurement of total area of inflammatory infiltrates in the liver. (*H*) Quantitative-PCR analysis of TNF-α mRNA expression in the liver. Average expression level in *Sh3bp2*$^{+/+}$ mice treated with DMSO was set as 1. (*I*) Serum TNF-α levels of GS-9973-treated or DMSO-treated *Sh3bp2*$^{+/+}$ and *Sh3bp2*$^{KI/KI}$ mice at 16 weeks old. Data are presented as mean ± SD. *$p < 0.05$. ANOVA with Tukey-Kramer post hoc test. ND = not detectable; NS = not significant.

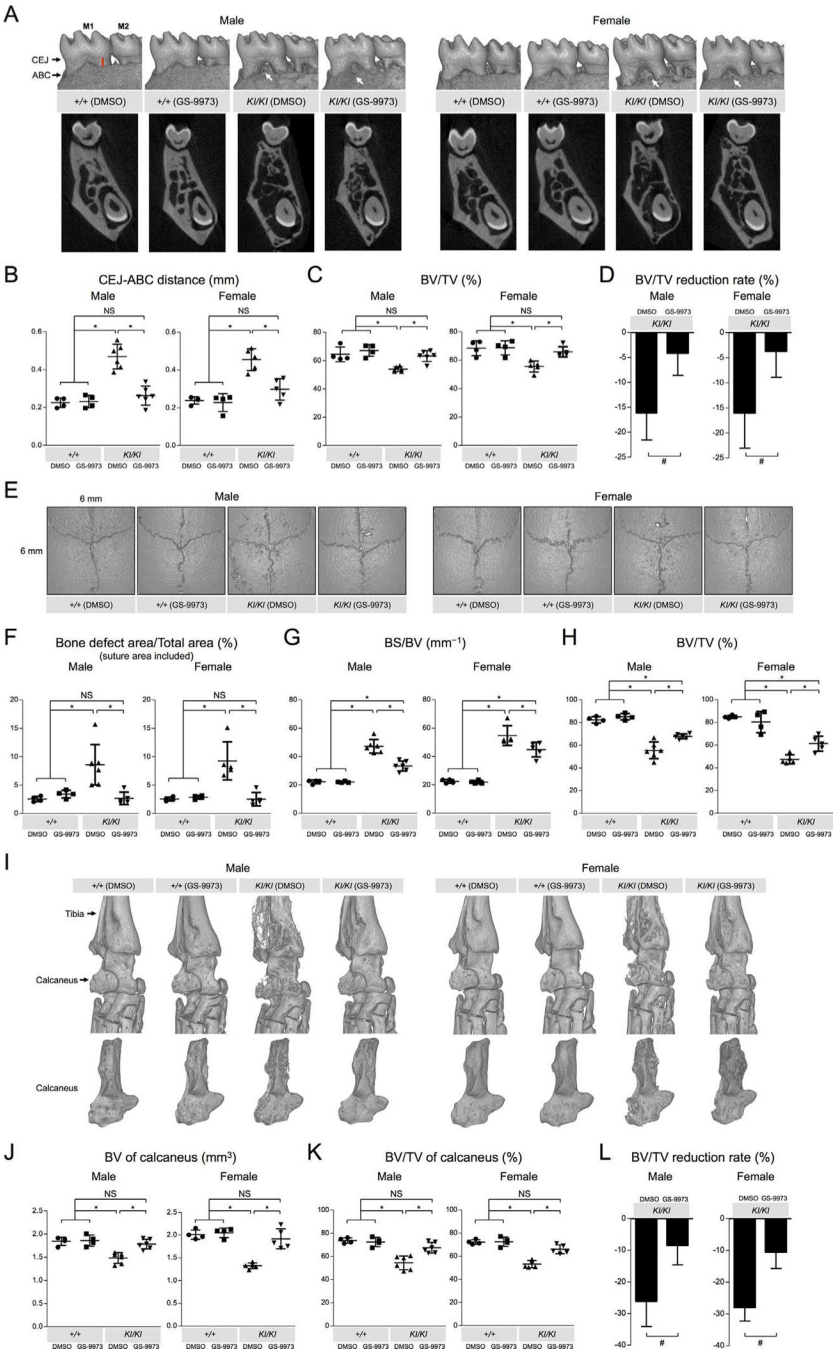

Fig. 2.

Decreased craniofacial bone erosion and ankle joint destruction in adult *Sh3bp2*$^{KI/KI}$ mice treated with GS-9973. (*A*) Reconstructed 3D μCT images of the mandibular bone (top) and reconstructed 2D μCT images showing the coronal plane at the center of the mandibular first molar (bottom) from 16-week-old *Sh3bp2*$^{+/+}$ and *Sh3bp2*$^{KI/KI}$ mice treated with GS-9973 or DMSO for 6 weeks. Black arrows indicate CEJ and ABC. Red line indicates the distance between CEJ and ABC. White arrows indicate erosion pits. (*B*) Quantitative measurement of the CEJ-ABC distance at the distal lingual surface of the mandibular first molar. (*C*) BV/TV.

Alveolar bone between roots of the mandibular first molar was segmented and subjected for analysis. (*D*) Reduction rate of alveolar BV/TV in *Sh3bp2*$^{KI/KI}$ mice treated with GS-9973 or DMSO relative to *Sh3bp2*$^{+/+}$ mice treated with DMSO. (*E*) Reconstructed μCT images of calvarial bone from GS-9973-treated or DMSO-treated 16-week-old *Sh3bp2*$^{+/+}$ and *Sh3bp2*$^{KI/KI}$ mice. Note that overall numbers and areas of erosion pits in GS-9973-treated *Sh3bp2*$^{KI/KI}$ mutant mice are decreased compared to DMSO-treated 16-weeks-old *Sh3bp2*$^{KI/KI}$ mice. (*F*) Quantitative measurement of calvarial bone erosion. Proportion (%) of bone erosion area including suture to total calvarial bone area (6 mm × 6 mm) was calculated. (*G*) BS/BV in the 6-mm × 6-mm area. (*H*) BV/TV in the 6-mm × 6-mm area. (*I*) 3D μCT images of the ankle joint (top) and calcaneus (bottom) from 16-week-old *Sh3bp2*$^{+/+}$ and *Sh3bp2*$^{KI/KI}$ mice treated with GS-9973 or DMSO. (*J, K*) BV and BV/TV of calcaneus. (*L*) Reduction rate of calcaneus BV/TV in *Sh3bp2*$^{KI/KI}$ mice treated with GS-9973 or DMSO relative to *Sh3bp2*$^{+/+}$ mice treated with DMSO. Data are presented as mean ± SD. **p* < 0.05. ANOVA with Tukey-Kramer post hoc test. #*p* < 0.05 with two-tailed *t* test. NS = not significant; M1 = first molar; M2 = second molar; CEJ = cementoenamel junction; ABC = alveolar bone crest; BV/TV = bone volume/tissue volume; BS/BV = bone surface/bone volume.